

## NOTES AND CORRESPONDENCE

# XBT Effects on the Global Ocean State Estimates Using a Coupled Data Assimilation System

You-Soon Chang<sup>1,\*</sup> and Shaoqing Zhang<sup>2</sup>

<sup>1</sup>*Department of Earth Science Education, Kongju National University, Kongju, South Korea*

<sup>2</sup>*Geophysical Fluid Dynamics Laboratory/NOAA, Princeton, NJ, USA*

Received 25 February 2016, revised 21 September 2016, accepted 23 September 2016

---

### ABSTRACT

The early 21<sup>st</sup> century experienced a transition in global ocean observing systems from the expendable bathythermograph (XBT) to the Argo. There has been a decrease in XBT observations, and a significant increase in Argo profiling floats in the global ocean. However, numerical XBT observation evaluations during this transition period have been under presented. This study investigates the XBT use effects on the global ocean observing systems using a coupled data assimilation model developed by the Geophysical Fluid Dynamics Laboratory (GFDL). Results show that the inclusion of XBT data significantly increases the accuracy of heat content and sea level change estimations during the pre-Argo period. During the Argo period, the amount of heat content correction by XBT assimilation is significantly weakened, especially in the upper ocean. However, it remains in the deeper oceans below 700 m depths, which is the residual effects of assimilating XBT data with the pre-Argo period. This study also confirms that although XBT only provides temperature observations mostly in the upper 700 m of the northern hemisphere, it can affect both the temperature and salinity fields of data assimilation systems, especially in the deep and southern oceans, which is also supported by the significant change in steric height.

Key words: Global ocean observing system, XBT, Argo, Data assimilation

Citation: Chang, Y. S. and S. Zhang, 2016: XBT effects on the global ocean state estimates using a coupled data assimilation system. *Terr. Atmos. Ocean. Sci.*, 27, 1019-1031, doi: 10.3319/TAO.2016.09.23.01

---

### 1. INTRODUCTION

An expendable bathythermograph (XBT) is a probe that measures the ocean temperature as it sinks through the ocean from research vessels, cargo or cruise ships. The greatest asset of the XBT is its lower cost and management effectiveness compared to a traditional Conductivity, Temperature, Depth (CTD) measurement. It had therefore, been widely used to observe upper ocean temperatures during the 20<sup>th</sup> century.

However, XBT data usage for global scale studies has two critical issues. One of these is the fall rate equation (FRE) problem. XBT relies on a FRE to estimate depth by recording the descending time because it does not have a pressure sensor. FRE has an error of about  $\pm 5$  m or 2%

depth that yields a significant uncertainty in temperature measurements (Goes et al. 2015a). Hanawa et al. (1995) first suggested a correction for XBT FRE biases, and many subsequent studies have continuously proven the negative impact of XBT biases on ocean climate studies (Kizu et al. 2005; Gouretski and Koltermann 2007; Domingues et al. 2008; Wijffels et al. 2008; Levitus et al. 2009; DiNezio and Goni 2011; Cowley et al. 2013; Goes et al. 2013; Cheng et al. 2014, 2015). So far, no agreement has been reached on how the XBT data should be corrected before it is used in climate studies. The XBT science team suggests careful reviews of all of the methods before a correction is chosen.

Another critical issue is the reduction in XBT observations in the 21<sup>st</sup> century. Figure 1 gives the yearly global XBT and Argo counts obtained from the latest World Ocean Database (WOD) version provided by the National Oceanographic Data Center (NODC) (Boyer et al. 2013). There is

---

\* Corresponding author  
E-mail: yschang@kongju.ac.kr

a significant decrease in the number of XBT observations after 2000. In 2012, only 14814 profiles were obtained, which is about 18% of the total number (83139 profiles) of XBT profiles in 1990. However, this decrease in the XBT observations is not a serious concern for the oceanographic and climate research community because the Argo array has rapidly increased instead, as shown in Fig. 1. The Argo array reached its initial target of operating 3000 robotic floats worldwide in 2007 (Roemmich et al. 2009).

As another important ocean observing system, the Tropical Atmospheric Ocean, Triangle Trans-Ocean Buoy Network (TAO/TRITON) has experienced a similar situation. Many TAO/TRITON buoys stopped and the number of observations decreased to about 40% since 2013. The number of observations by TAO buoys temporarily recovered to 80% after mid-2014 although the number of TRITON buoys has recently reduced (Tollefson 2014). Nevertheless, the TAO/TRITON array has its own merits when compared with the Argo float. Meridional and temporal sampling of Argo profiles is somewhat larger than the TAO/TRITON array. Autonomous Argo floats also tend to move away from the equator due to the equatorial near surface current. Therefore, several studies have evaluated the impacts of the TAO/TRITON array on assimilation systems using a variety of operational and research applications (Fujii et al. 2015; Xue et al. 2015). They pointed out the severe effects of the recent decrease in TAO/TRITON data on the accuracies of the analyzed fields, which make issuing reliable forecast statements such as El Niño-Southern Oscillation (ENSO) evolution more difficult, even in the Argo period.

Meanwhile, XBT observation system evaluation has been underrepresented. As previously mentioned, only the quality control (QC) issue of XBT bias is being actively investigated by many studies. The possible role of biases in XBT data to assimilating models have also been analyzed in previous studies (Giese et al. 2011; Goes et al. 2015a, b). This study therefore focuses only on the XBT data effects on global oceanic state estimations during the transition period from XBT to Argo by employing an observing system experiment (OSE). The OSE involves the systematic withholding of different observation types from a data assimilating model to assess the degradation in the quality of analysis or forecasting when that observation type is excluded (Oke et al. 2009). Previous studies demonstrated the impact of Argo using traditional OSEs (Balmaseda et al. 2007; Oke and Schiller 2007; Smith and Haines 2009). Recently, near-real time OSEs are tested in parallel with operational ocean forecast systems developed by Mercator Ocean, Met Office, Canadian consortium, Bluelink, Collecte Localisation Stellites (CLS), Japan Meteorological Agency (JMA), European Centre for Medium-Range Weather Forecasts (ECMWF), along with other groups (Lea 2012; Lea et al. 2014; Oke et al. 2015). However, they did not treat the XBT array as a major data component that is withheld from their assimilating systems.

This study focuses mainly on quantifying the upper and deeper ocean changes when only an XBT observation platform is withheld from a data assimilation model for the period 1993 - 2006. The next section describes the assimilation model characteristics and the methodology used in this study. In section 3, we assess how the XBT measurements may affect the assimilation fields in time. The summary and discussion are presented in the final section.

## 2. MODEL AND METHODS

This study uses the Ensemble Coupled Data Assimilation (ECDA) system developed by the Geophysical Fluid Dynamics Laboratory (GFDL). ECDA is based on a fully coupled climate model, Climate Model version 2.1 (CM2.1) that is one of GFDL Intergovernmental Panel on Climate Change (IPCC) models (Delworth et al. 2006). The CM2.1 ocean component is Modular Ocean Model version 4 (MOM4) with  $1^\circ$  by  $1^\circ$  horizontal resolution telescoping to a  $1/3^\circ$  meridional spacing near the equator. It has 50 vertical levels and there are 22 levels of 10 m thicknesses in the top 220 m, which is adequate to simulate global XBT arrays. We may use a higher resolution configuration to investigate XBT's effect on a regional scale, but the scope of this study is limited to the global scale. More details such as parameterizations and specified characteristics of the MOM4 can be found in Griffies et al. (2005) and Gnanadesikan et al. (2006).

The ECDA assimilation module employs an ensemble Kalman filter under a local least square framework considering temperature and salinity covariance (Anderson 2003). Recently, Chang et al. (2013) published comprehensive assessments of the ECDA system, and Zhang et al. (2014) emphasized the benefit of the coupled data assimilation approach based on biased twin experiment. This study adopted the same assimilation module as previous studies as a base model for OSE. Details of the data assimilation algorithms

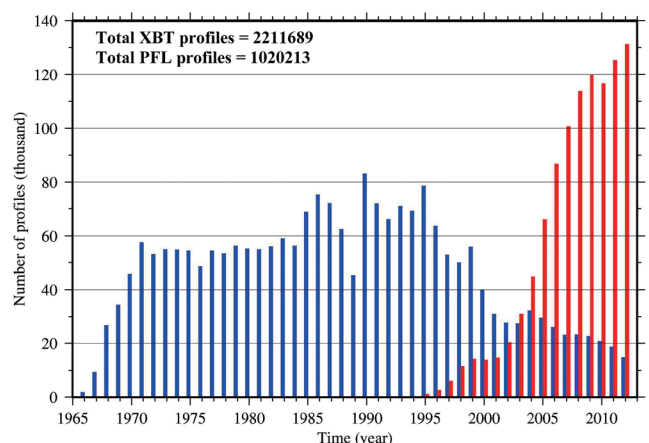


Fig. 1. Temporal distribution of (blue bar) XBT and (red bar) Argo profiles in the global ocean. (Color online only)

can be originally found in Zhang et al. (2007).

In order to investigate the XBT effects on the ECDA system in the early 21<sup>st</sup> century, an assimilation system was integrated from 1993 - 2006. Since the ECDA is based on a fully coupled model, atmospheric data were constrained by existing atmospheric reanalyses (air temperature and wind speed) from 6-h mean National Center for Environmental Prediction/Department of Energy (NCEP/DOE) reanalyses at each grid point (Kanamitsu et al. 2002). For the surface temperature, the gridded Optimal Interpolation Sea Surface Temperature (OISST) was also assimilated into the ECDA (Reynolds et al. 2007). For subsurface ocean temperature and salinity observations, this study basically used every available “observed full depth” profiles from the WOD 2009 (Boyer et al. 2009). Before assimilation, conventional QC had been carried out based on the NODC and Argo QC manual (Boyer and Levitus 1994; Wong et al. 2006). Salinity offset and pressure sensor errors discovered in some Argo floats have been removed based on delayed mode information (Chang et al. 2009). As previously mentioned, FRE XBT biases have also been corrected using the traditional methods in Hanawa et al. (1995) and Kizu et al. (2005).

Two simulations were conducted in this study. One assimilated all of the in-situ profiles (referred to as ALL), and the other used all of the profiles except for the XBT (referred to as no\_XBT). Figure 2 shows the spatial distribution and number of XBT profiles used in the ALL simulation in this study. As previously mentioned, we observed

that the total XBT observational cast significantly decreases in time. In 1993, the first assimilation year, there were a total of 63082 profiles for the entire world ocean. The number of profiles conducted decreased by 42000 over 13 years, therefore, only 21082 profiles were available for use for assimilation in the last assimilation year, 2006. The number of Argo profiles increased after 2006, while the number of XBT did not rapidly change after 2000. Because the study period is in the early 21<sup>st</sup> century, simulation results up to 2006 were conducted. It should also be noted that most of the XBT profiles measured upper ocean temperature in the northern hemisphere.

Two simulations were initiated from January 1993 using the same restart file from the respective analysis using the previous result (Chang et al. 2013) and the same periods were analyzed. This study focused on the variability in the upper ocean heat content per unit area, which is defined as:

$$Q = \rho C_p \int_z \theta(z) dz \quad (1)$$

where  $\rho$  is the water density,  $C_p$  is the specific heat capacity of seawater, and  $\theta$  is the potential temperature. The integration depths specified in this study were 50, 300, 700, and 5000 m.

In order to check density variation from temperature and salinity changes, we also estimated steric sea level (SL) by separating the thermal and haline component as:

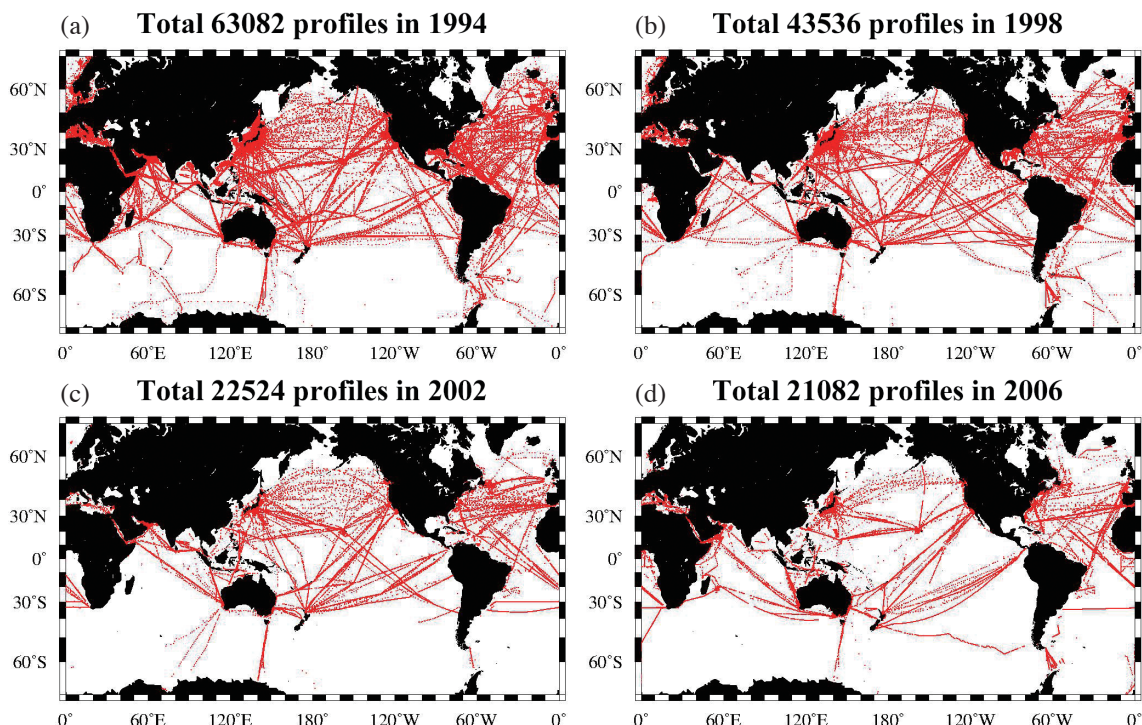


Fig. 2. Spatial distribution and number of XBT profiles used in the ALL simulation of (a) 1994, (b) 1998, (c) 2002, and (d) 2006. (Color online only)

$$SL = \frac{1}{\rho_0} \int_{H_2}^{H_1} \rho(T, \bar{S}) dz + \frac{1}{\rho_0} \int_{H_2}^{H_1} \rho(\bar{T}, S) dz \quad (2)$$

where  $\rho_0$  is the reference density and the over-bar denotes the time-average value. We calculated the thermosteric and halosteric contributions of the two different levels (0 - 700 m, 700 m - bottom).

This study used Archiving, Validation and Interpretation of Satellite Oceanographic data (AVISO) as an independent dataset for verification. The TOPEX/Poseidon, Jason-1, ERS-1/2, and Envisat satellite measurements on  $1/3^\circ$  by  $1/3^\circ$  grid points were merged, and the data has been updated weekly since 1993 (Dibarboure et al. 2008). Data were averaged into monthly mean values and spatially interpolated to the same ECDA grid.

As a reference dataset for the direct comparison of temperature and salinity at model each layer, this study used the Ensemble version 3 (EN3) that is an objective analyzed (OA) product of T - S provided by Met Office Hadley Center (Ingleby and Huddleston 2007). EN3 makes a suitable dataset since it provides monthly T - S fields with 42 vertical levels covering the early 21<sup>st</sup> century study period, 1993 - 2006. We also used various versions of the World Ocean Atlas (WOA01, WOA05, WOA09, and WOA13; hereafter WOAs) provided by NODC. EN3 and WOAs were also linearly interpolated to match the ECDA grid for comparison purposes.

### 3. RESULTS

Figure 3 shows the difference between the assimilated

heat contents at the upper 700 m depth (hereafter HC700) of two experiments (no\_XBT minus ALL simulation). The HC700 estimation was chosen because most XBT profiles have maximum sampling depths of around 700 m. Within 2 years after initialization, XBT assimilation effects on HC700 are clearly found, especially along the subtropical area,  $20^\circ\text{N(S)} - 40^\circ\text{N(S)}$ , and in most parts of the Indian Oceans, where the XBT effect is more than  $4 \times 10^{10} \text{ J m}^{-2}$  (Fig. 3a). In general, warm differences are depicted around the North Pacific when no XBT data are assimilated. Cold differences are dominant near the Gulf stream meandering region, South Atlantic, and the east coast of Australia. It is known that the base model of this study, CM2.1, has a systematic warm bias around the subsurface layer associated with the subtropical gyre circulations (Delworth et al. 2006). We confirmed that XBT assimilation effects are especially found along the subtropical gyres, but it is not easy to identify the close relationship between the spatial pattern of difference and systematic error of the base model. The spatial patterns in Fig. 3 also changed with time, which implies that the assimilation of XBT profiles induces either warm or cold biases in the upper ocean ECDA status due to the dynamic processes in the fully-coupled assimilation system. A prominent example is that there are significant differences in the southern ocean even though XBT observations are limited to the northern hemisphere along the ship tracks (see Fig. 2). Differences in HC700 between the two simulations are also reduced with time after 2002 because large amounts of Argo profiles are continuously applied to the assimilation system, as mentioned in Fig. 1.

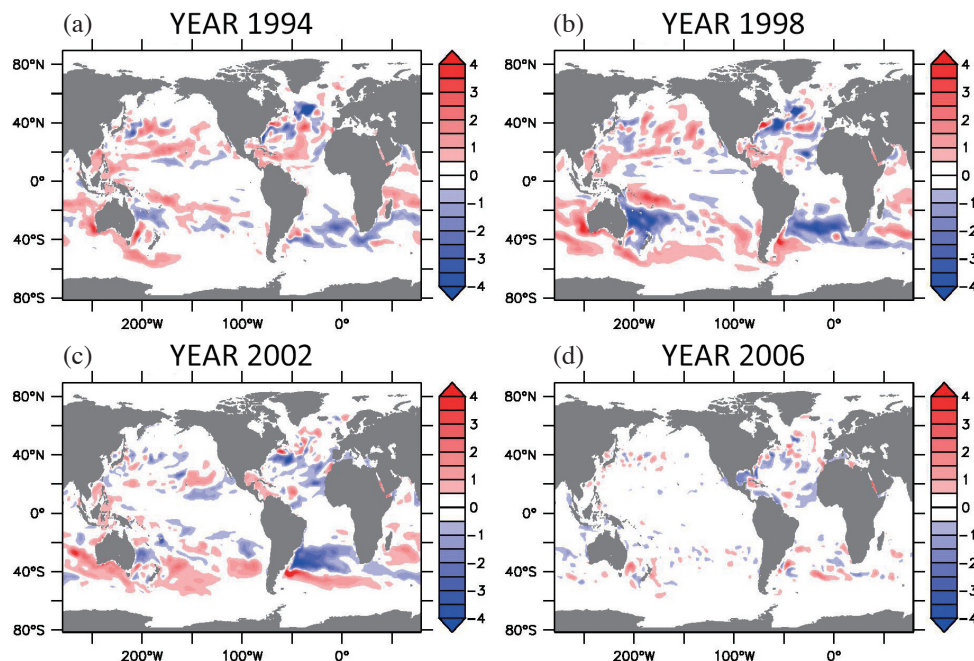


Fig. 3. Difference in heat content (unit:  $\text{J} \times 10^{10} \text{ m}^{-2}$ ) over 0 - 700 m depth between no\_XBT and ALL simulation in (a) 1994, (b) 1998, (c) 2002, and (d) 2006. (Color online only)

Since we implemented ensemble calculations through the ECDA system, we can estimate the statistical significance of the upper ocean heat content difference by comparing ensemble spreads of each experiment. Figure 4 provides a time-series of all twelve-member ensemble spreads for the temperature correction. The difference in global mean temperature corrections between the two experiments [ALL (black lines in Fig. 4) and no\_XBT (red lines in Fig. 4)] is shown larger than each ensemble spread. Therefore, we can conclude that the difference in the ensemble mean heat contents between the two experiments shown in Fig. 3 is meaningful considering the deviation in each ensemble member during the assimilation procedure. Figure 5 also represents the significance level for the mean difference in heat content

over a 0 - 700 m depth for 14 years between no\_XBT and ALL simulations. We can check areas that show significant differences between no\_XBT and ALL assimilations within a 95% significant level. As previously mentioned, it is interesting that there are significant differences in the southern ocean even though XBT observations are limited in the northern hemisphere along the ship tracks.

In order to quantify the XBT effects on assimilated fields in time, this study estimates the evolution of the root mean square difference (RMSD) in global heat contents for the no\_XBT experiment with respect to ALL assimilation in Fig. 6. As previously noted, two simulations were initialized in January 1993. Therefore, the maximum difference does not appear immediately in 1993, which is related to

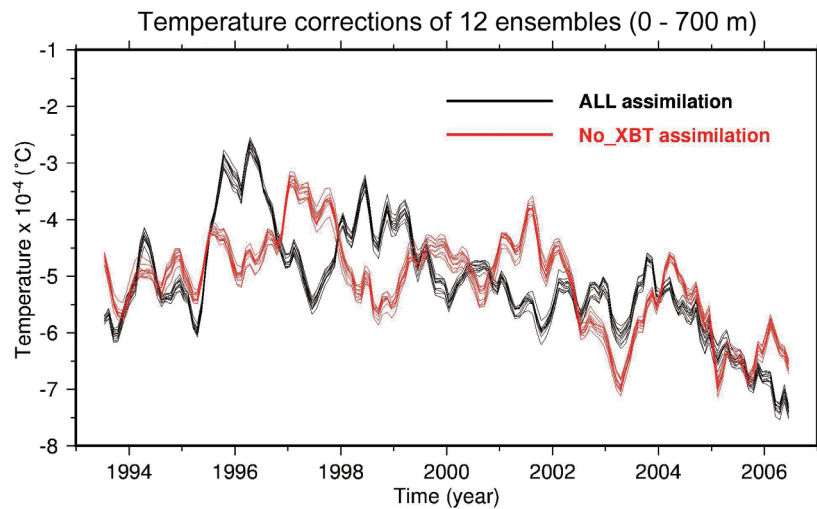


Fig. 4. Twelve-member ensemble spreads for the temperature correction of the global ocean averaged from 0 - 700 m depth. Black (red) lines denote the ALL (no\_XBT) assimilation results. (Color online only)

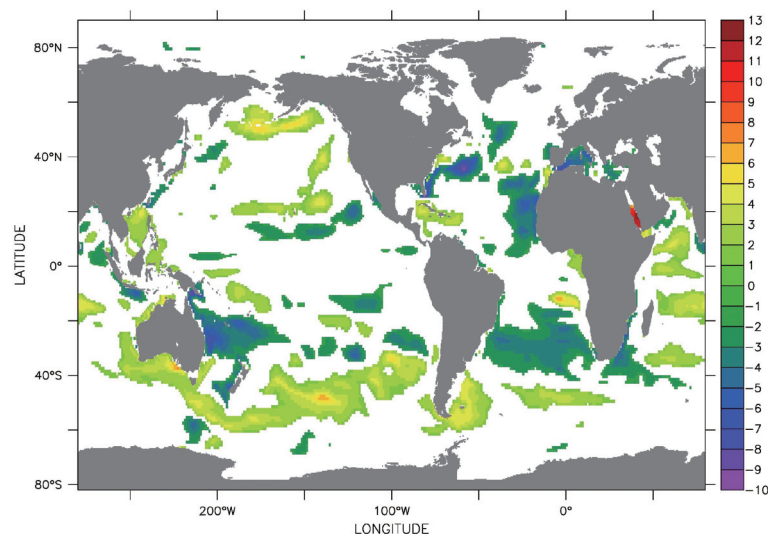


Fig. 5. T values larger than 95% significant limits for mean differences of heat content over 0 - 700 m depth between no\_XBT and ALL simulations. (Color online only)

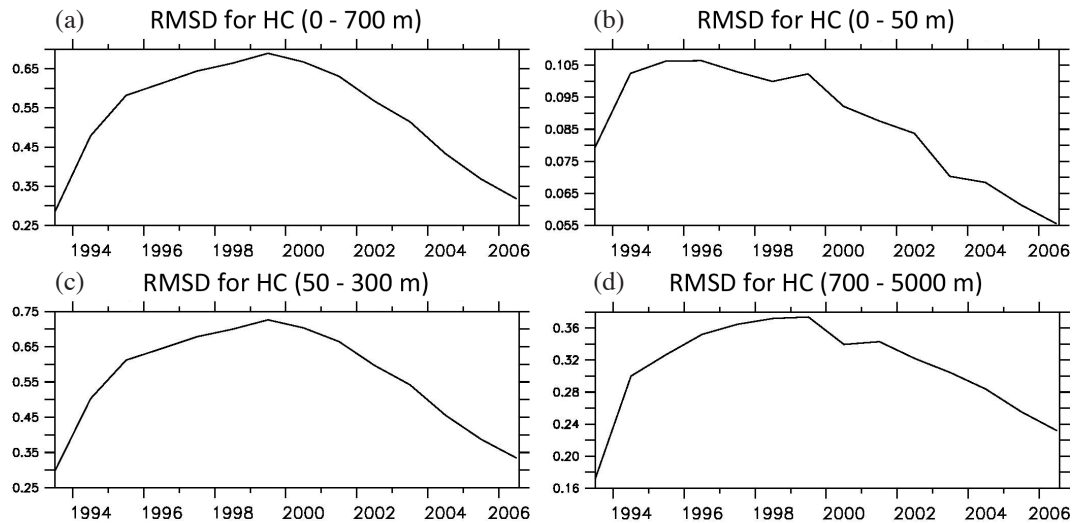


Fig. 6. RMSD (unit:  $\text{J} \times 10^9 \text{ m}^{-2}$ ) change between global heat content from no\_XBT and ALL assimilation for 1993 - 2006 over (a) 0 - 700 m, (b) 0 - 50 m, (c) 50 - 300 m, and (d) 700 - 5000 m depth.

assimilation adjustment time and it is also sensitive to the ocean layer. At the surface, the maximum difference is found in 1996 (Fig. 6b), while it is delayed up to 1999 and below the subsurface layer (Figs. 6c, d).

As shown by previous results in Fig. 3, XBT effects HC700 of ECDA significantly decreasing after 2000 due to the increased number of Argo profiles and decreased number of XBT profiles (Fig. 6a), but the periods when RMSDs decrease down to the original values are different for each layers. Around the surface layer, integrated from the surface to only a 50-m depth (Fig. 6b), XBT effects decrease the most rapidly (RMSD decreases back to the original values in around 2002) which is related to their interaction with SST and atmospheric increments in the coupled assimilation system. However, for the deeper layer below 700 m (Fig. 6d), the XBT effect remains even after the Argo period in 2006, which is more than  $0.22 \times 10^9 \text{ J m}^{-2}$  of the averaged heat content difference. This result emphasizes the importance of accurate oceanic initialization especially for the deep ocean, which also affects long-term climate prediction.

Figure 7 shows sea surface height (SSH) anomaly correlations between observed satellite data and assimilation, and the root mean square error (RMSE) with satellite data for 1993 - 2000. We calculated the correlation and RMSE for the ALL assimilation and no\_XBT assimilation experiments and compared the results. We used the AVISO gridded data as an independent observation for the assessment of assimilation. As mentioned in the previous study (Chang et al. 2013), ECDA shows high correlations within a 95% confidence level around the tropical and subtropical Pacific, eastern North Pacific, and the subpolar North Atlantic (Fig. 7a). The RMSE of SSH with respect to AVISO is generally large around the western boundary and high latitude southern ocean (Fig. 7b). No\_XBT assimilation shows

similar spatial patterns (Figs. 7c, d) with ALL assimilation. For the correlation difference (Fig. 7e), XBT significantly improves SSH variability especially around the subtropical area (correlation coefficient degradation from XBT withholding is more than 0.2 within a 95% confidence level), even though the XBT effects on some Antarctic areas are negative. Judging from both correlation and RMSE, we can conclude that there is general degradation when we withhold XBT data from the data assimilation system for 1993 - 2000 (see overall decrease of correlation and increase RMSE in Figs. 7e, f). This result indicates that XBT data assimilation corrects sea level height by changing density fields in the ECDA system, even though altimetry information is not used for the ECDA system. As we can expect, no significant improvement is obtained for ALL assimilation compared to no\_XBT simulation during the Argo period (2001 - 2006), which is obviously related to the decreased (increased) number of XBT (Argo) data during the Argo period (not shown).

Since ECDA employs a multivariate scheme considering temperature and salinity (T - S) covariance function during the assimilation procedure, we can expect that XBT temperature only profiles directly affect the assimilated salinity fields as well (Zhang et al. 2007). Figure 8 shows the time series of potential temperature and salinity averaged over the global ocean at 5 different model layers.

At the surface layer shown in Figs. 8a, b, both ALL and no\_XBT have systematic warm and fresh biases with respect to EN3 and WOAs. However, the differences between the two assimilations (ALL and no\_XBT simulations) are very small, when the mean differences among EN3 and WOAs are compared. For example, the differences in the fresh bias between ALL and no\_XBT experiments is about 0.05 psu, but they both still show significant fresh biases

of more than 0.1 psu when EN3 and WOAs are compared. In the current coupled assimilation system, strong oceanic surface and atmospheric assimilation from gridded OISST and NCEP/DOE atmospheric reanalysis prevents XBT data from significantly changing the ocean status at the surface layer. However, it does not mean that XBTs have no effect on surface variables in the assimilation system. In Fig. 7, we have already shown that XBTs have significant effects on the variations of sea level in the assimilation system.

At a 205-m depth in Figs. 8c, d, overall differences between the two experiments seem to be meaningful. When XBT was withheld, warm bias tends to be larger (about  $0.1^{\circ}\text{C}$ ) than ALL experiment, especially for early the simulated periods, 1993 - 1999 (Fig. 8c). This mean difference of about  $0.1^{\circ}\text{C}$  is comparable or even larger than the system-

atic ECDA warm biases during the same period (Chang et al. 2013). In addition, this difference is reduced when large amounts of Argo profiles are used in the assimilation system after 2000. However, this bias reduction due to XBT cannot be shown in the salinity field. Saline biases are prominent in the ALL experiment, while no\_XBT tends to be in line with EN3, which means XBT temperature data leads to saline biases around this layer. This result suggests that the salinity correction calculated from temperature observations through T - S covariance relationship could degrade the salinity field in the data assimilation system. Interestingly, differences are dominant during 1997 - 2005. This result shows that T - S bias reductions do not occur simultaneously, which may be related to the T - S covariance relationship within the dynamic process of the fully coupled data assimilation

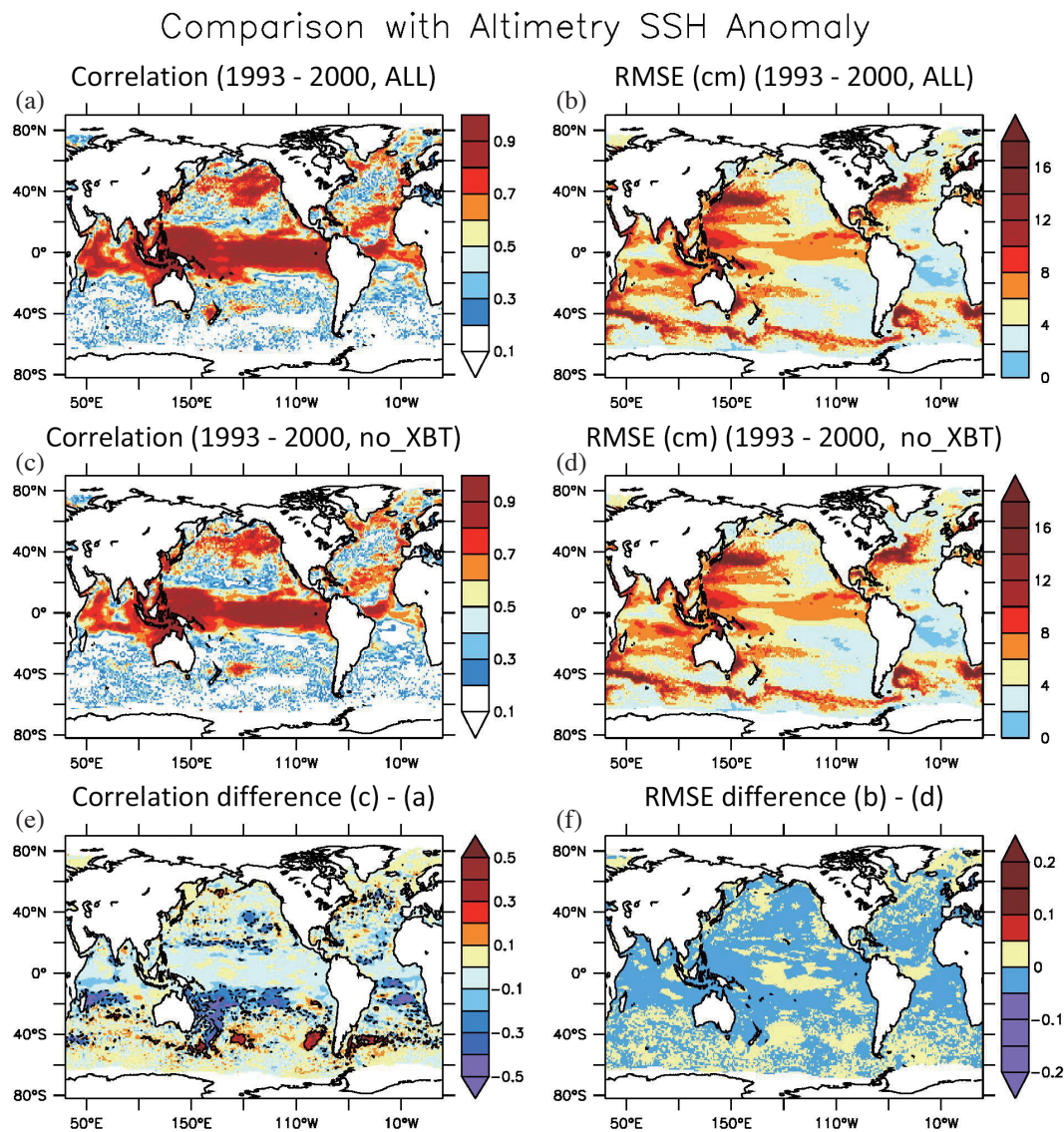


Fig. 7. (a) Anomaly correlation and (b) RMSE between ALL assimilation and AVISO altimetry for 1993 - 2000. (c) and (d) represents correlation and RMSE between no\_XBT assimilation and AVISO altimetry during the same periods. (e) and (f) are their differences. Correlation coefficient lower than 95% significant levels are shown in white. (Color online only)

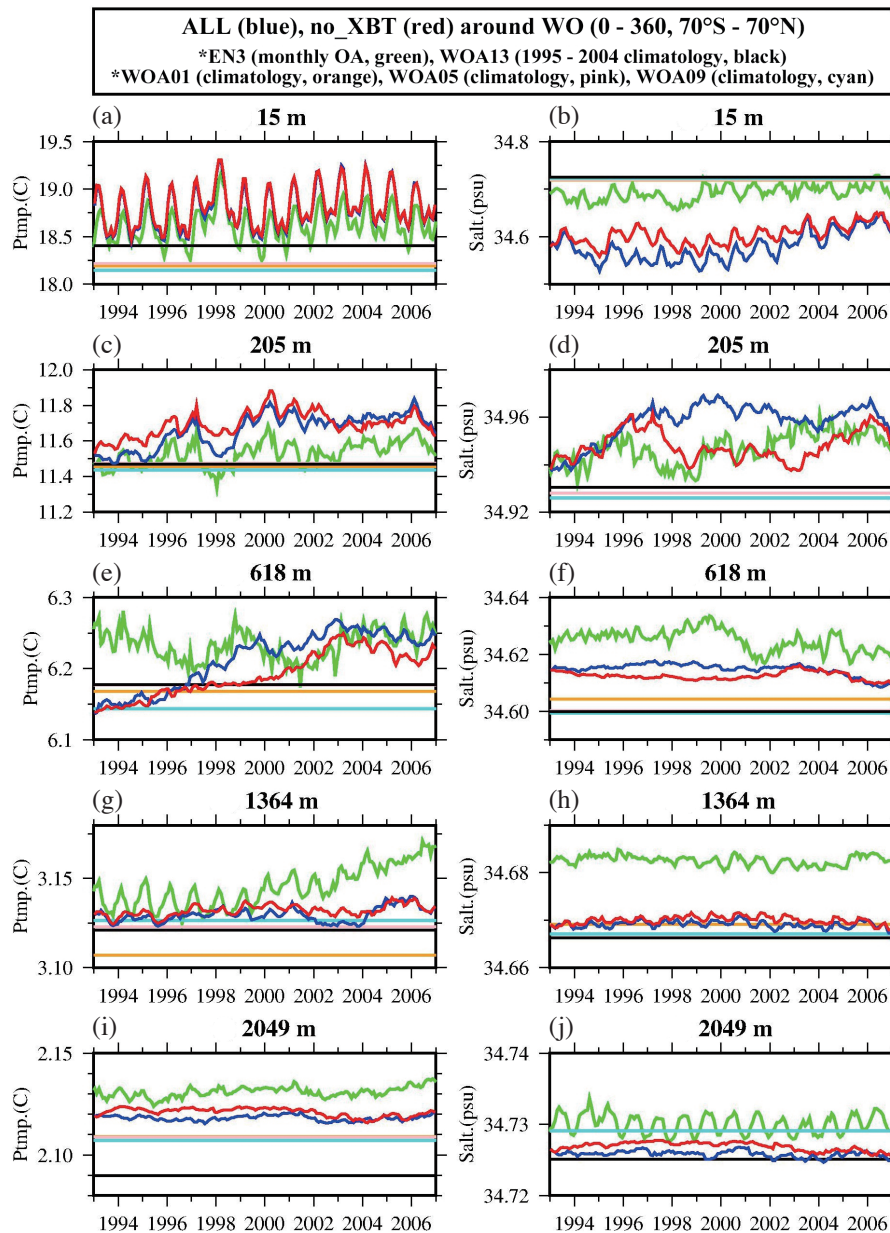


Fig. 8. Time series of (left panels) potential temperature and (right panels) salinity averaged over the global ocean ( $0 - 360^{\circ}$ ,  $70^{\circ}\text{S} - 70^{\circ}\text{N}$ ) at 15, 205, 618, 1364, and 2049 m depth, respectively. Thick blue and red lines indicate the assimilation results from ALL and no\_XBT experiments. Thin green lines denote corresponding value ranges from EN3 and other straight lines are the annual mean values of WOA climatologies (WOA01, WOA05, WOA09, and WOA13). (Color online only)

system. At a 618-m depth (Figs. 8e, f), temperature differences remain even after the Argo period. When XBT is withheld, cold and fresh biases remain when the ALL assimilation is compared, but T - S ranges of both simulations are located between mean values of EN3 and WOAs, so we cannot conclude that these biases are significant.

For deep oceans in 1364 and 2049 m depths, the differences between two experiments are not clearly shown. However, we cannot simply conclude that XBT has no significant effects on the deep layers, because T - S variability is generally very small in the deep ocean. The small amount

of T - S change due to XBT withholding could be due to the effect of some impact for the deep ocean. Mean ECDA values are also located between EN3 and WOAs. Compared to existing climatologies, EN3 shows abnormal warm and saline differences in a 618-m depth and in the deeper layers, so we cannot determine which one is accurate and correct the T - S ranges around the deep ocean accordingly.

As shown in Fig. 2, most XBT were observed in the northern hemisphere along the ship tracks. Meanwhile, significant spatial differences in HC700 are found between the two assimilations, even in the southern ocean, which might

be directly related to the XBT effect around the area between the equator and  $30^{\circ}\text{S}$ . We also checked similar T - S time series at each model layer, which is shown in Fig. 8, except for those averaged only over the northern and southern oceans (not shown). The amount of T - S reduction and temporal changes due to XBT withholding is almost the same between the two hemispheres, which confirms that XBT affects the T - S fields of the data assimilation system in the deep and southern oceans, although XBT is a temperature only constraint source mostly deployed in the upper 700 m of the north of  $30^{\circ}\text{S}$ .

In order to investigate the difference between the two experiments in detail, this study additionally estimated and compared steric height changes averaged over 9 different major ocean basins, because global averages would not be able to differentiate between different water masses from different locations. We also separated the thermosteric and halosteric components of two different levels (0 - 700 m, 700 m - bottom) in order to determine the dominant component in the region. Study area were selected based on previous studies (Xue et al. 2011; Chang et al. 2013).

Thermosteric heights around most ocean basins show significant interannual variability. Increasing trends can be found, especially in the tropical western Pacific (blue line in Fig. 9a) and in most Atlantic areas (Figs. 9c, g, h). As for the halosteric component, it exhibits little interannual variability compared to the thermosteric height. The global ocean exhibits a decreasing trend for the halosteric contribution (green line in Fig. 9i), which is mainly affected by the salinity change in the Equatorial Eastern Pacific (Fig. 9b), North Eastern Pacific (Fig. 9e), and in most areas of the Atlantic Ocean (Figs. 9c, g, h). All these results correspond well to the recent study estimated from various assimilated and objective analyses ensembles (Storto et al. 2015).

Surprisingly, it is shown that the mean difference in halosteric heights between the two assimilations is comparable with that of the thermosteric contributions. We can easily infer significant differences in thermosteric height between the two experiments in the upper ocean due to the large amount of direct constrains in the XBT profiles. However, this study reveals that XBT profiles can affect steric height by changing the salinity fields due to the multivariate scheme considering

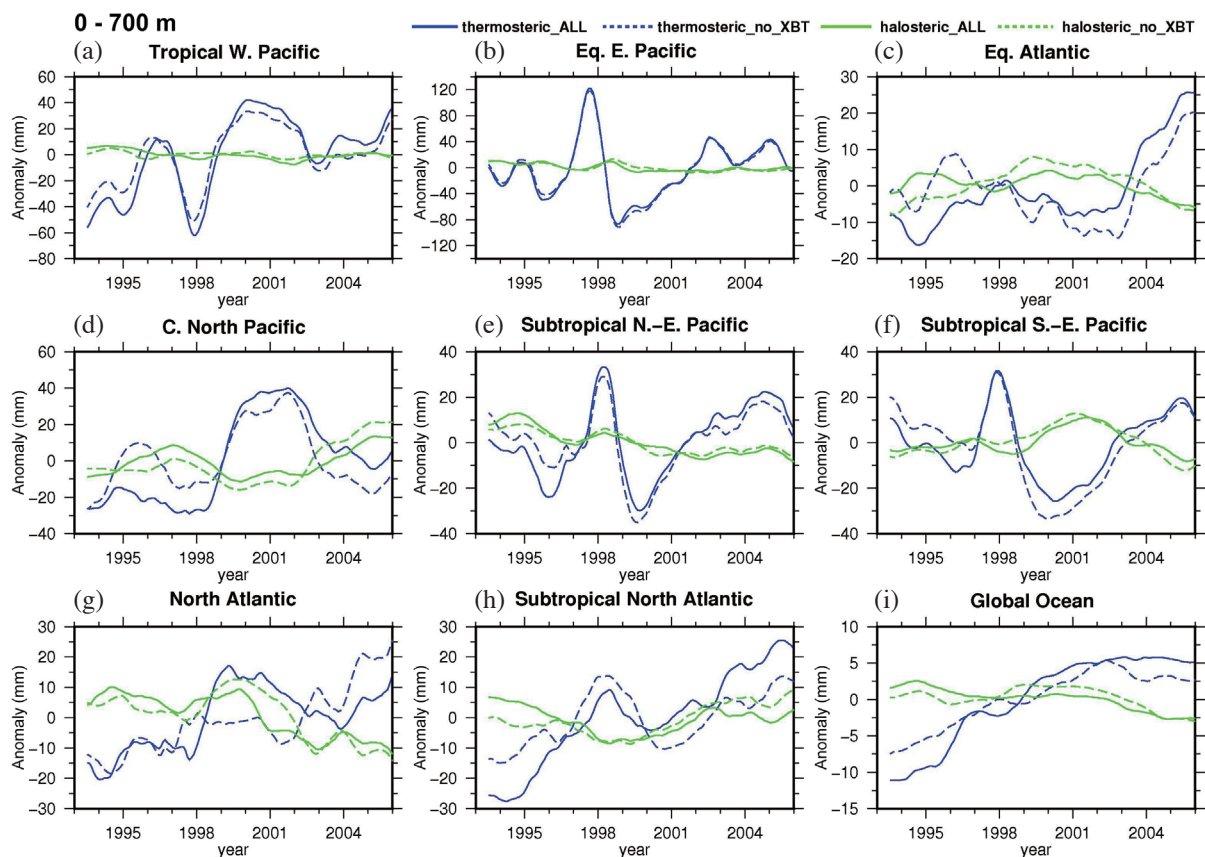


Fig. 9. Time-series of (blue lines) thermosteric and (green lines) halosteric sea level anomalies estimated from (solid lines) ALL and (dotted lines) no\_XBT assimilation in the upper ocean (0 - 700 m depth) of (a) tropical western Pacific ( $130 - 190^{\circ}\text{E}$ ,  $20^{\circ}\text{S} - 20^{\circ}\text{N}$ ), (b) equatorial eastern Pacific ( $210 - 270^{\circ}\text{E}$ ,  $5^{\circ}\text{S} - 5^{\circ}\text{N}$ ), (c) equatorial Atlantic ( $310 - 10^{\circ}\text{E}$ ,  $10^{\circ}\text{S} - 10^{\circ}\text{N}$ ), (d) central North Pacific ( $180 - 220^{\circ}\text{E}$ ,  $20 - 40^{\circ}\text{N}$ ), (e) subtropical northeast Pacific ( $220 - 270^{\circ}\text{E}$ ,  $5 - 25^{\circ}\text{N}$ ), (f) subtropical southeast Pacific ( $220 - 280^{\circ}\text{E}$ ,  $5^{\circ}\text{S} - 25^{\circ}\text{N}$ ), (g) subpolar North Atlantic ( $280 - 350^{\circ}\text{E}$ ,  $30 - 60^{\circ}\text{N}$ ), (h) subtropical North Atlantic ( $280 - 360^{\circ}\text{E}$ ,  $5 - 25^{\circ}\text{N}$ ), and (i) the global Ocean ( $0 - 360^{\circ}\text{E}$ ,  $70^{\circ}\text{S} - 70^{\circ}\text{N}$ ). All time-series have been smoothed by a 12-month filter. (Color online only)

T - S covariance function in the ECDA system that have already been addressed in a previous section. The salinity fields are also modulated by assimilating the XBT temperature data indirectly through the change in ocean circulation fields. This tendency can still be found in the deep ocean, below 700 m depths (Fig. 10). In this layer the difference is relatively large particularly in the North Atlantic (Fig. 10g), which might be related to the deep ocean response from XBT withholding in the assimilation system. We checked the temporal distribution of the number of XBT and Argo profiles around these regions (not shown). Even though the number of total profiles and initial Argo deployment periods are different from each other, it is common that XBT (Argo) generally decreases (increases) in time. Therefore, it is not easy to find any close relationship between the temporal evolution of steric height change and the number of XBT or Argo observations. Further studies to explain the deep ocean response mechanism from the upper ocean temperature data constraints in detail will be necessary.

**4. SUMMARY AND DISCUSSION**

This study investigated the influences of global XBT profiles on a data assimilation system. To address this issue, a traditional OSE was designed using GFDL’s ECDA for

the period 1993 - 2006 when the primary global observation system was changed from XBT to Argo. Two simulations assimilating all in situ profiles (ALL) and all except for XBT (no\_XBT) were conducted.

The results show that the XBT effect on HC700 calculated from the assimilative ocean field is estimated to be more than  $4 \times 10^{10} \text{ J m}^{-2}$ , especially along the subtropical areas, but they show little consistent differences in either warm or cold biases. Spatial patterns of heat content difference between ALL and no\_XBT simulations change with time, and they are rapidly weakened during the Argo period. This study also showed that deeper ocean tends to retain the temperature constraints memory from XBT profiles in the 1990s, even after the number of Argo profiles were increased in the early 20<sup>th</sup> century. XBT significantly affects the temperature, but also the corresponding salinity and density fields of the ECDA that considers the T - S covariance function. Differences in the steric height below 700 m depths are observed especially around the Atlantic Ocean.

Even though we reported that the XBT’s effects are rapidly weakened during the Argo period, we cannot conclusively state that the XBT is unnecessary for describing the current ocean status in the 21<sup>st</sup> century. This research is focused only on the global scale. Current high density XBT transects are designed to investigate the detailed boundary

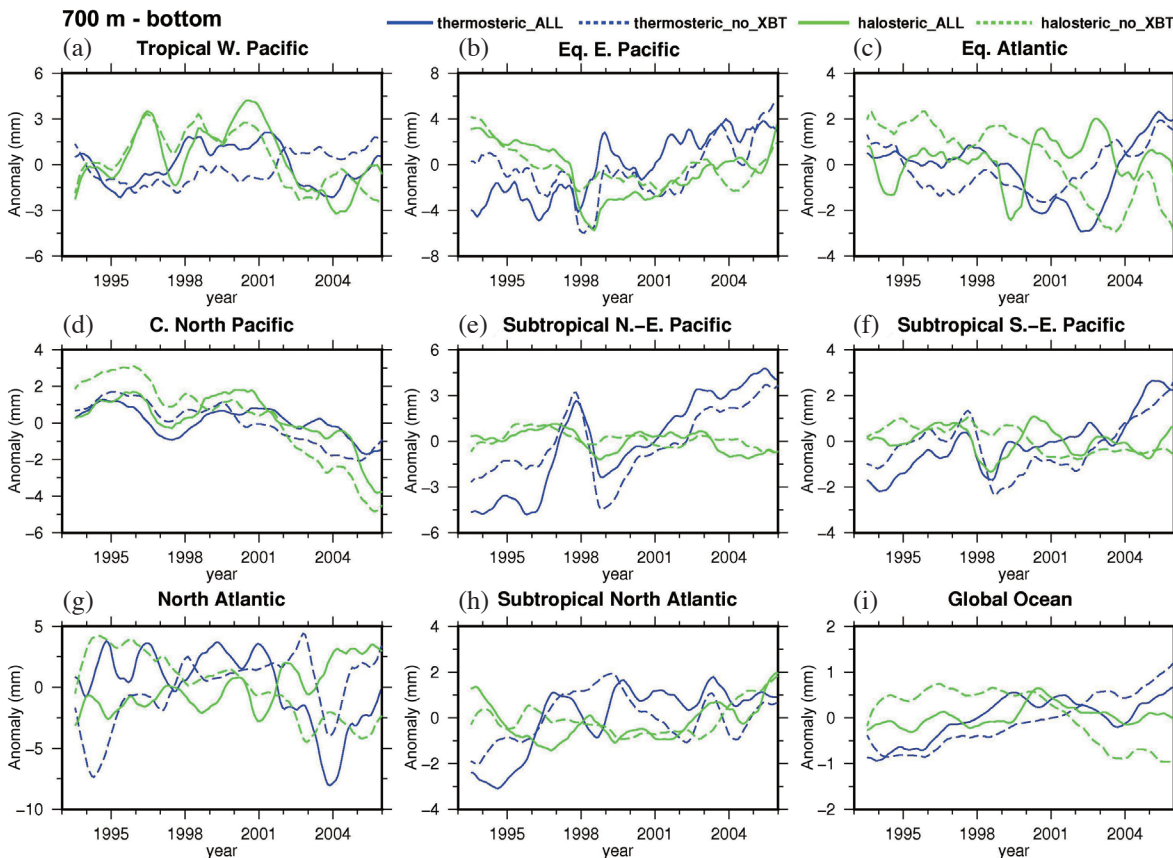


Fig. 10. The same as Fig. 9 except for the deeper ocean (700 m - bottom). (Color online only)

current, mesoscale features and possibly to measure instantaneous events that the Argo cannot measure. Therefore, the possible regional effects of the XBT array should be evaluated using a high-resolution model with a high density XBT array [see high density XBT transects provided by Scripps (<http://www-hrx.ucsd.edu>) or AOML (Atlantic Oceanographic and Meteorological laboratory, <http://www.aoml.noaa.gov/phod/hdenxht/index.php>)].

The traditional OSE based on the data denial experiment using only one given data assimilation system has a limitation. Assimilation models are largely affected by systematic base model errors. In order to overcome this limitation, we needed to use a validated assimilation model for OSEs. Therefore, this study used a state-of-the-art GFDL's ECDA system whose quality had already been evaluated by previous studies (Zhang et al. 2007, 2014; Chang et al. 2013). However, all models are imperfect and still have large errors and uncertainties. In addition, the ECDA used in this study is based on a fully coupled model. Most ocean data assimilation systems employ optimal interpolation or variational methods based on ocean-only models. Therefore, quantitative ranges in HC700 differences between the two simulations presented in this study could be dependent on the ECDA system specifics. In other words, model-sensitive error bounds on the XBT impact on ocean analysis cannot be identified unless many different systems are used.

This study showed that XBT plays a role in constraining the overall quality of temperature, salinity, sea level, and steric height. This result may be dependent on the ECDA system specifics. Other models could show possible different changes for other oceanic and atmospheric variables such as current, transport and heat flux when XBT is withheld. Therefore, multi-model OSEs are necessary to provide a comprehensive conclusion for the global and regional XBT simulation experiments in the future. This study did not provide detailed information about the deep ocean change mechanisms associated with XBT withholding in the assimilation system. We expect that a comprehensive investigation focused on explaining why the deeper layer is affected by XBT and determining which areas or water masses play important roles will follow this study.

**Acknowledgements** We acknowledge the NODC for providing publicly available World Ocean Database including XBT and Argo profiles. This data helped make this study possible. We appreciate the Three Anonymous Reviewers for their constructive feedback that helped to improve our manuscript. This work (2014R1A2A2A01003486) was supported by the Mid-career Researcher Program through National Research Foundation grant funded by the Korean Ministry of Science, ICT and Future Planning.

## REFERENCES

- Anderson, J. L., 2003: A local least squares framework for ensemble filtering. *Mon. Weather Rev.*, **131**, 634-642, doi: 10.1175/1520-0493(2003)131<0634:ALLSFF>2.0.CO;2. [[Link](#)]
- Balmaseda, M., D. Anderson, and A. Vidard, 2007: Impact of Argo on analyses of the global ocean. *Geophys. Res. Lett.*, **34**, L16605, doi: 10.1029/2007GL030452. [[Link](#)]
- Boyer, T. P. and S. Levitus, 1994: Quality control and processing of historical oceanographic temperature, salinity, and oxygen data. NOAA Technical Report NESDIS 81, U.S. Dept. of Commerce, National Oceanic and Atmospheric Administration, National Environmental Satellite, Data, and Information Service, Washington, D.C., 64 pp.
- Boyer, T. P., J. I. Antonov, O. K. Baranova, H. E. Garcia, D. R. Johnson, R. A. Locarnini, A. V. Mishonov, T. D. O'Brien, D. Seidov, I. V. Smolyar, and M. M. Zweng, 2009: World Ocean Database 2009, NOAA Atlas NESDIS 66, U.S. Gov. Printing Office, Wash., D.C., 216 pp.
- Boyer, T. P., J. I. Antonov, O. K. Baranova, C. Coleman, H. E. Garcia, A. Grodsky, D. R. Johnson, R. A. Locarnini, A. V. Mishonov, T. D. O'Brien, C. R. Paver, J. R. Reagan, D. Seidov, I. V. Smolyar, and M. M. Zweng, 2013: World Ocean Database 2013, NOAA Atlas NESDIS 72, Silver Spring, MD, 209 pp.
- Chang, Y. S., A. J. Rosati, S. Zhang, and M. J. Harrison, 2009: Objective analysis of monthly temperature and salinity for the world ocean in the 21st century: Comparison with World Ocean Atlas and application to assimilation validation. *J. Geophys. Res.*, **114**, C02014, doi: 10.1029/2008JC004970. [[Link](#)]
- Chang, Y. S., S. Zhang, A. Rosati, T. L. Delworth, and W. F. Stern, 2013: An assessment of oceanic variability for 1960-2010 from the GFDL ensemble coupled data assimilation. *Climate Dyn.*, **40**, 775-803, doi: 10.1007/s00382-012-1412-2. [[Link](#)]
- Cheng, L., J. Zhu, R. Cowley, T. Boyer, and S. Wijffels, 2014: Time, probe type, and temperature variable bias corrections to historical expendable bathythermograph observations. *J. Atmos. Ocean. Technol.*, **31**, 1793-1825, doi: 10.1175/JTECH-D-13-00197.1. [[Link](#)]
- Cheng, L., J. Abraham, G. Goni, T. Boyer, S. Wijffels, R. Cowley, V. Gouretski, F. Reseghetti, S. Kizu, S. Dong, F. Bringas, M. Goes, L. Houpert, J. Sprintall, and J. Zhu, 2015: XBT Science: Assessment of instrumental biases and errors. *Bull. Amer. Meteorol. Soc.*, **97**, 924-933, doi: 10.1175/BAMS-D-15-00031.1. [[Link](#)]
- Cowley, R., S. Wijffels, L. Cheng, T. Boyer, and S. Kizu, 2013: Biases in expendable bathythermograph data: A new view based on historical side-by-side comparisons. *J. Atmos. Ocean. Technol.*, **30**, 1195-1225, doi: 10.1175/JTECH-D-12-00127.1. [[Link](#)]
- Delworth, T., A. J. Broccoli, A. Rosati, R. J. Stouffer, V.

Anderson, J. L., 2003: A local least squares framework for

- Balaji, J. A. Beesley, W. F. Cooke, K. W. Dixon, J. Dunne, K. A. Dunne, J. W. Durachta, K. L. Findell, P. Ginoux, A. Gnanadesikan, C. T. Gordon, S. M. Griffies, R. Gudgel, M. J. Harrison, I. M. Held, R. S. Hemler, L. W. Horowitz, S. A. Klein, T. R. Knutson, P. J. Kushner, A. R. Langenhorst, H. C. Lee, S. J. Lin, J. Lu, S. L. Malyshev, P. C. D. Milly, V. Ramaswamy, J. Russell, M. D. Schwarzkopf, E. Shevliakova, J. J. Sirutis, M. J. Spelman, W. F. Stern, M. Winton, A. T. Wittenberg, B. Wyman, F. Zeng, and R. Zhang, 2006: GFDL's CM2 global coupled climate models. Part I: Formulation and simulation characteristics. *J. Climate*, **19**, 643-674, doi: 10.1175/JCLI3629.1. [[Link](#)]
- Dibarboure, G., O. Lauret, F. Mertz, and V. Rosmorduc, 2008: SSALTO/DUACS User Handbook: (M)SLA and (M)ADT Near-Real Time and Delayed Time Products, Rep. CLS-DOS-NT06.034, Collect. Localisation Satell., Ramonville Saint-Agne, France.
- DiNezio, P. N. and G. J. Goni, 2011: Direct evidence of a changing fall-rate bias in XBTs manufactured during 1986-2008. *J. Atmos. Ocean. Technol.*, **28**, 1569-1578, doi: 10.1175/JTECH-D-11-00017.1. [[Link](#)]
- Domingues, C. M., J. A. Church, N. J. White, P. J. Gleckler, S. E. Wijffels, P. M. Barker, and J. R. Dunn, 2008: Improved estimates of upper-ocean warming and multi-decadal sea-level rise. *Nature*, **453**, 1090-1093, doi: 10.1038/nature07080. [[Link](#)]
- Fujii, Y., J. Cummings, Y. Xue, A. Schiller, T. Lee, M. A. Balmaseda, E. Rémy, S. Masuda, G. Brassington, O. Alves, B. Cornuelle, M. Martin., P. Oke, G. Smith, and X. Yang, 2015: Evaluation of the Tropical Pacific Observing System from the ocean data assimilation perspective. *Q. J. R. Meteorol. Soc.*, **141**, 2481-2496, doi: 10.1002/qj.2579. [[Link](#)]
- Giese, B. S., G. A. Chepurin, J. A. Carton, T. P. Boyer, and H. F. Seidel, 2011: Impact of bathythermograph temperature bias models on an ocean reanalysis. *J. Climate*, **24**, 84-93, doi: 10.1175/2010JCLI3534.1. [[Link](#)]
- Gnanadesikan, A., K. W. Dixon, S. M. Griffies, V. Balaji, M. Barreiro, J. A. Beesley, W. F. Cooke, T. L. Delworth, R. Gerdes, M. J. Harrison, I. M. Held, W. J. Hurlin, H. C. Lee, Z. Liang, G. Nong, R. C. Pacanowski, A. Rosati, J. Russell, B. L. Samuels, Q. Song, M. J. Spelman, R. J. Stouffer, C. O. Sweeney, G. Vecchi, M. Winton, A. T. Wittenberg, F. Zeng, R. Zhang, and J. P. Dunne, 2006: GFDL's CM2 global coupled climate models. Part II: The baseline ocean simulation. *J. Climate*, **19**, 675-697, doi: 10.1175/JCLI3630.1. [[Link](#)]
- Goes, M., G. Goni, and K. Keller, 2013: Reducing biases in XBT measurements by including discrete information from pressure switches. *J. Atmos. Ocean. Technol.*, **30**, 810-824, doi: 10.1175/JTECH-D-12-00126.1. [[Link](#)]
- Goes, M., M. Baringer, and G. Goni, 2015a: The impact of historical biases on the XBT-derived meridional overturning circulation estimates at 34°S. *Geophys. Res. Lett.*, **42**, 1848-1855, doi: 10.1002/2014GL061802. [[Link](#)]
- Goes, M., G. Goni, and S. Dong, 2015b: An optimal XBT-based monitoring system for the South Atlantic meridional overturning circulation at 34°S. *J. Geophys. Res.*, **120**, 161-181, doi: 10.1002/2014JC010202. [[Link](#)]
- Gouretski, V. and K. P. Koltermann, 2007: How much is the ocean really warming? *Geophys. Res. Lett.*, **34**, L01610, doi: 10.1029/2006GL027834. [[Link](#)]
- Griffies, S. M., A. Gnanadesikan, K. W. Dixon, J. P. Dunne, R. Gerdes, M. J. Harrison, A. Rosati, J. L. Russell, B. L. Samuels., M. J. Spelman, M. Winton, and R. Zhang, 2005: Formulation of an ocean model for global climate simulations. *Ocean Sci.*, **1**, 45-79, doi: 10.5194/os-1-45-2005. [[Link](#)]
- Hanawa, K., P. Rual, R. Bailey, A. Sy, and M. Szabados, 1995: A new depth-time equation for Sippican or TSK T-7, T-6 and T-4 expendable bathythermographs (XBT). *Deep-Sea Res. Part I-Oceanogr. Res. Pap.*, **42**, 1423-1451, doi: 10.1016/0967-0637(95)97154-Z. [[Link](#)]
- Ingleby, B. and M. Huddleston, 2007: Quality control of ocean temperature and salinity profiles — Historical and real-time data. *J. Mar. Syst.*, **65**, 158-175, doi: 10.1016/j.jmarsys.2005.11.019. [[Link](#)]
- Kanamitsu, M., W. Ebisuzaki, J. Woolen, S. K. Yang, J. J. Hnilo, M. Fiorino, and G. L. Potter, 2002: NCEP-DOE AMIP-II reanalysis (R-2). *Bull. Amer. Meteorol. Soc.*, **83**, 1631-1643, doi: 10.1175/BAMS-83-11-1631. [[Link](#)]
- Kizu, S., H. Yoritaka, and K. Hanawa, 2005: A new fall-rate equation for T-5 Expendable Bathythermograph (XBT) by TSK. *J. Oceanogr.*, **61**, 115-121, doi: 10.1007/s10872-005-0024-4. [[Link](#)]
- Lea, D., 2012: Observation Impact Statements for operational ocean forecasting. Forecasting R&D Technical Report no. 568, Met Office, 57 pp.
- Lea, D. J., M. J. Martin, and P. R. Oke, 2014: Demonstrating the complementarity of observations in an operational ocean forecasting system. *Q. J. R. Meteorol. Soc.*, **140**, 2037-2049, doi: 10.1002/qj.2281. [[Link](#)]
- Levitus, S., J. I. Antonov, T. P. Boyer, R. A. Locarnini, H. E. Garcia, and A. V. Mishonov, 2009: Global ocean heat content 1955-2008 in light of recently revealed instrumentation problems. *Geophys. Res. Lett.*, **36**, L07608, doi: 10.1029/2008GL037155. [[Link](#)]
- Oke, P. R. and A. Schiller, 2007: Impact of Argo, SST, and altimeter data on an eddy-resolving ocean reanalysis. *Geophys. Res. Lett.*, **34**, L19601, doi: 10.1029/2007GL031549. [[Link](#)]
- Oke, P. R., M. A. Balmaseda, M. Benkiran, J. A. Cummings, E. Dombrowsky, Y. Fujii, S. Guinehut, G. Larnicol, P. Y. Le Traon, and M. J. Martin, 2009: Observing system

- evaluations using GODAE systems. *Oceanography*, **22**, 144-153, doi: 10.5670/oceanog.2009.72. [[Link](#)]
- Oke, P. R., G. Larnicol, Y. Fujii, G. C. Smith, D. J. Lea, S. Guinehut, E. Remy, M. A. Balmaseda, T. Rykova, D. Surcel-Colan, M. J. Martin, A. A. Sellar, S. Mulet, and V. Turpin, 2015: Assessing the impact of observations on ocean forecasts and reanalyses: Part 1, Global studies. *J. Operational Oceanogr.*, **8**, s49-s62, doi: 10.1080/1755876X.2015.1022067. [[Link](#)]
- Reynolds, R. W., T. M. Smith, C. Liu, D. B. Chelton, K. S. Casey, and M. G. Schlax, 2007: Daily high-resolution-blended analyses for sea surface temperature. *J. Climate*, **20**, 5473-5496, doi: 10.1175/2007JCLI1824.1. [[Link](#)]
- Roemmich, D., G. C. Johnson, S. Riser, R. Davis, J. Gilson, W. B. Owens, S. L. Garzoli, C. Schmid, and M. Ignaszewski, 2009: The Argo Program: Observing the global ocean with profiling floats. *Oceanography*, **22**, 34-43, doi: 10.5670/oceanog.2009.36. [[Link](#)]
- Smith, G. C. and K. Haines, 2009: Evaluation of the  $S(T)$  assimilation method with the Argo dataset. *Q. J. R. Meteorol. Soc.*, **135**, 739-756, doi: 10.1002/qj.395. [[Link](#)]
- Storto, A., S. Masina, M. Balmaseda, S. Guinehut, Y. Xue, T. Szekely, I. Fukumori, G. Forget, Y. S. Chang, S. A. Good, A. Köhl, G. Vernieres, N. Ferry, K. A. Peterson, D. Behringer, M. Ishii, S. Masuda, Y. Fujii, T. Toyoda, Y. Yin, M. Valdivieso, B. Barnier, T. Boyer, T. Lee, J. Gourrion, O. Wang, P. Heimback, A. Rosati, R. Kovach, F. Hernandez, M. J. Martin, M. Kamachi, T. Kuragano, K. Mogensen, O. Alves, K. Haines, and X. Wang, 2015: Steric sea level variability (1993-2010) in an ensemble of ocean reanalyses and objective analyses. *Climate Dyn.*, 21 pp, doi: 10.1007/s00382-015-2554-9. [[Link](#)]
- Tollefson, J., 2014: El Niño tests forecasters. *Nature*, **508**, 20-21, doi: 10.1038/508020a. [[Link](#)]
- Wijffels, S. E., J. Willis, C. M. Domingues, P. Barker, N. J. White, A. Gronell, K. Ridgway, and J. A. Church, 2008: Changing expendable bathythermograph fall rates and their impact on estimates of thermosteric sea level rise. *J. Climate*, **21**, 5657-5672, doi: 10.1175/2008JCLI2290.1. [[Link](#)]
- Wong, A., R. Keeley, and T. Carvel, 2006: Argo data management quality control manual, version 2.2. Rep. arum-04-01, Argo Data Manage., Brest, France.
- Xue, Y., B. Huang, Z. Z. Hu, A. Kumar, C. Wen, D. Behringer, and S. Nadiga, 2011: An assessment of oceanic variability in the NCEP climate forecast system reanalysis. *Climate Dyn.*, **37**, 2511-2539, doi: 10.1007/s00382-010-0954-4. [[Link](#)]
- Xue, Y., C. Wen, X. Yang, D. Behringer, A. Kumar, G. Vecchi, A. Rosati, and R. Gudgel, 2015: Evaluation of tropical Pacific observing systems using NCEP and GFDL ocean data assimilation systems. *Climate Dyn.*, 1-26, doi: 10.1007/s00382-015-2743-6. [[Link](#)]
- Zhang, S., M. J. Harrison, A. Rosati, and A. Wittenberg, 2007: System design and evaluation of coupled ensemble data assimilation for global oceanic climate studies. *Mon. Weather Rev.*, **135**, 3541-3564, doi: 10.1175/MWR3466.1. [[Link](#)]
- Zhang, S., Y. S. Chang, X. Yang, and A. Rosati, 2014: Balanced and coherent climate estimation by combining data with a biased coupled model. *J. Climate*, **27**, 1302-1314, doi: 10.1175/JCLI-D-13-00260.1. [[Link](#)]